Effect of dipole-quadrupole Robinson mode coupling upon the beam response to radio-frequency phase noise

R. A. Bosch and K. J. Kleman

Synchrotron Radiation Center, University of Wisconsin-Madison, 3731 Schneider Dr., Stoughton, Wisconsin 53589, USA

(Received 15 May 2006; published 12 September 2006)

In an electron storage ring, coupling between dipole and quadrupole Robinson oscillations modifies the spectrum of longitudinal beam oscillations driven by radio-frequency (rf) generator phase noise. In addition to the main peak at the resonant frequency of the coupled dipole Robinson mode, another peak occurs at the resonant frequency of the coupled quadrupole mode. To describe these peaks analytically for a quadratic synchrotron potential, we include the dipole and quadrupole modes when calculating the beam response to generator noise. We thereby obtain the transfer function from generator-noise phase modulation to beam phase modulation with and without phase feedback. For Robinson-stable bunches confined in a synchrotron potential with a single minimum, the calculated transfer function agrees with measurements at the Aladdin 800-MeV electron storage ring. The transfer function is useful in evaluating phase feedback that suppresses Robinson oscillations in order to obtain quiet operation of an infrared beam line.

DOI: 10.1103/PhysRevSTAB.9.094401 PACS numbers: 29.27.Bd, 29.20.Dh, 41.75.Ht

I. INTRODUCTION

In an electron storage ring, phase noise from the radio-frequency (rf) generator excites longitudinal beam motion in which all bunches oscillate in unison, termed Robinson oscillations. When coupling of the dipole and quadrupole Robinson modes is negligible, white rf-generator noise excites oscillations whose amplitude is largest at the dipole Robinson frequency [1,2]. Because of coupling between the dipole and quadrupole Robinson modes [3,4], the spectrum of beam oscillations also displays a peak at the frequency of the coupled quadrupole Robinson mode [5,6]. The spectrum of the longitudinal beam oscillations (''beam phase noise'') provides a useful diagnostic of the coupled dipole and quadrupole Robinson modes.

The power transmitted through an infrared beam line is affected by Robinson oscillations, which cause oscillations of the electron beam current, energy, direction of propagation, and transverse position. The latter two oscillations result from transverse momentum and position dispersion at the beam line's source point. For a typical setup of the Aladdin infrared spectromicroscopy beam line, the computed power variations from these four oscillations are in the approximate ratio 1:200:1400:7600 [7]. This suggests that oscillations of the electron beam transverse position are the most important mechanism by which Robinson oscillations affect the Aladdin infrared beam line. Since the infrared beam line performs Fourier transform infrared spectroscopy with a moving mirror, an audio frequency oscillation of the power through the beam line produces the same signal on the detector as a spectral peak [8].

When commissioning low-emittance operation of the Aladdin electron storage ring, Robinson oscillations at frequencies around 3 kHz prevented useful operation of the infrared beam line. Additional filtering in the rf system and the use of a low-noise master oscillator improved the beam line data. Quiet operation of the beam line was achieved by using phase feedback to further suppress Robinson oscillations [9–13]. To predict the effect of such feedback, an analytical model of the Robinson oscillations is useful.

In this article, we analytically describe driven Robinson oscillations in a quadratic synchrotron potential well. Dipole-quadrupole-mode coupling, radiation damping, and feedback are modeled. We calculate the transfer function from generator-noise phase modulation to beam phase modulation.

We compare the calculated transfer function with the measured transfer function, using a passive harmonic cavity to vary the coupled quadrupole Robinson frequency. For Robinson-stable beams in a synchrotron potential with a single minimum, good agreement is obtained. The modification of the transfer function (and also the beam phase noise spectrum) from dipole-quadrupole-mode coupling and feedback is well described. In cases where parasitic coupled-bunch instability is not suppressed by the harmonic cavity, the measured height of the coupled-quadrupole peak is consistent with the beam's energy spread exceeding the natural value.

For Robinson-unstable beams and double-well synchrotron potentials, the experimental transfer function differs from the analytical model. For these cases, which violate the assumptions of the analytical model, macroparticle simulations provide a more accurate description of phase noise and its suppression by feedback [6,12,13].

II. EFFECT OF EXTERNAL PHASE NOISE AND FEEDBACK UPON THE BEAM

Consider stable operation of an electron storage ring powered by an rf cavity with rf-generator phase modulation from noise and feedback. In addition to the powered cavity (''Cavity 1''), a passive harmonic cavity may also be present [5,6,14–17]. We assume all rf buckets are filled equally, so that transient beam loading [18] may be neglected. Consider a small phase modulation at angular frequency Ω, where Ω is small compared to the angular rf frequency ω_g:

$$\Psi \exp(-i\Omega t) = (\psi_g + \psi_f)\exp(-i\Omega t). \tag{1}$$

Here, Ψ is the complex amplitude of the modulation, which is the sum of generator noise ψ_g and phase feedback ψ_f. The rf-generator phase modulation causes longitudinal oscillations of the beam electrons where all bunches move in unison. Within a single bunch, we follow Krinsky and Wang [15] by describing an electron's longitudinal position with a coordinate ϕ that equals zero for a synchronous electron, increases towards the head of the bunch, and varies between $-\pi$ and π around the ring. We denote the average phase oscillation of all electrons in the bunch as

$$\bar{\phi}(t) = \Phi \exp(-i\Omega t). \tag{2}$$

We now determine the amplitude of the beam oscillation caused by an rf-generator phase modulation, using the notation of Refs. [5,16] in which the voltage $V(t)$ is the accelerating rf voltage, positive when electrons are accelerated. In this notation, the synchronous phase angle ψ_1 is measured from the peak rf voltage, equaling $\pi/2$ for an electron that gains no energy from the rf cavity. Our definition of the synchronous phase is the complement of the definition used by some authors.

Consider a time coordinate where the synchronous times are $t = 2\pi n/\omega_g$ for integral n. The equivalent rf-generator current of magnitude i_{g1}, with phase modulation, is [16]

$$i_{g1}(t) = i_{g1}\cos[\omega_g t + \pi - \theta_{f1} + \Psi\exp(-i\Omega t)]. \tag{3}$$

The angle θ_{f1} is the angle by which the generator current lags the sinusoidal beam current component at frequency ω_g. The perturbation of the generator current from the phase modulation is

$$\begin{aligned}\Delta i_{g1}(t) &= i_{g1}\Psi\exp(-i\Omega t)\sin(\omega_g t - \theta_{f1}) \\ &= \frac{i_{g1}\Psi}{2i}[e^{i(\omega_g t-\theta_{f1}-\Omega t)} - e^{-i(\omega_g t-\theta_{f1}+\Omega t)}].\end{aligned} \tag{4}$$

Let the powered cavity have resonant angular frequency ω_1 near to the rf-generator frequency ω_g, impedance at resonance R_1, quality factor Q_1, and tuning angle $\phi_1 \equiv \tan^{-1}[2Q_1(\omega_g - \omega_1)/\omega_1]$. At the frequency ω_g, its impedance is $R_1\cos\phi_1\exp(i\phi_1)$. Our definition of tuning angle is the same as that used by Sands [19] and Marchand [20], and the negative of that used by Wilson [21]. The values R_1 and Q_1 describe the effective impedance of the loaded cavity, equaling $1/(1+\beta_1)$times the unloaded values, where β_1 is the rf coupling coefficient. In our notation, R_1 is the resistance of the equivalent parallel resistor-inductor-capacitor (*RLC*) circuit describing the cavity, equaling one-half of the ''linac'' definition of impedance [21].

We define sideband tuning angles by $\phi_{1\pm} \equiv \tan^{-1}[2Q_1(\omega_g \pm \Omega - \omega_1)/\omega_1]$, so that the powered-cavity impedance at frequencies $\omega_g \pm \Omega$ is $R_1\cos\phi_{1\pm}\exp(i\phi_{1\pm})$. Since $Z(-\omega) = Z*(\omega*)$, the perturbation of the cavity voltage from the phase modulation is

$$\begin{aligned}\Delta V(t) = \frac{i_{g1}R_1\Psi}{2i}&[e^{i(\omega_g t-\theta_{f1}-\Omega t)}\cos\phi_{1-}e^{-i\phi_{1-}} \\ &- e^{-i(\omega_g t-\theta_{f1}+\Omega t)}\cos\phi_{1+}e^{i\phi_{1+}}].\end{aligned} \tag{5}$$

The smoothed voltage perturbation experienced by an electron with longitudinal coordinate ϕ at time t is

$$\begin{aligned}\Delta V(\phi,t) = \frac{i_{g1}R_1\Psi\exp(-i\Omega t)}{2i}&\\ \times[e^{-iM\phi}e^{-i\theta_{f1}}\cos\phi_{1-}e^{-i\phi_{1-}}&\\ - e^{iM\phi}e^{i\theta_{f1}}\cos\phi_{1+}e^{i\phi_{1+}}],&\end{aligned} \tag{6}$$

where M is the number of bunches. Thus, we have the Fourier series representation $\Delta V(\phi,t) = \exp(-i\Omega t)\sum_{n=\pm M}\Delta V_n e^{in\phi}$, where

$$\begin{aligned}\Delta V_M &= \frac{-i_{g1}R_1\Psi}{2i}e^{i\theta_{f1}}\cos\phi_{1+}e^{i\phi_{1+}}, \\ \Delta V_{-M} &= \frac{i_{g1}R_1\Psi}{2i}e^{-i\theta_{f1}}\cos\phi_{1-}e^{-i\phi_{1-}}.\end{aligned} \tag{7}$$

The generator current is related to the powered-cavity peak voltage V_{T1} by Eq. (12) of Ref. [16]:

$$\begin{aligned}V_{T1}\cos(\omega_g t + \psi_1) = -R_1[&i_{g1}\cos\phi_1\cos(\omega_g t - \theta_{f1} - \phi_1) \\ &+ 2IF_1\cos\phi_1\cos(\omega_g t - \phi_1)].\end{aligned} \tag{8}$$

Here, $I > 0$ is the magnitude of the ring's average current and $F_1 \equiv F_{\omega_g} = \exp[-(\omega_g\sigma_t)^2/2]$ is the bunch form factor at frequency ω_g for rms bunch length σ_t, i.e., the bunch form factor in Cavity 1. Therefore,

$$\begin{aligned}\Delta V_M &= \frac{\Psi}{2i}\frac{\cos\phi_{1+}e^{i\phi_{1+}}}{\cos\phi_1 e^{i\phi_1}}(V_{T1}e^{-i\psi_1} + 2IR_1F_1\cos\phi_1 e^{i\phi_1}), \\ \Delta V_{-M} &= -\frac{\Psi}{2i}\frac{\cos\phi_{1-}e^{-i\phi_{1-}}}{\cos\phi_1 e^{-i\phi_1}} \\ &\quad\times(V_{T1}e^{i\psi_1} + 2IR_1F_1\cos\phi_1 e^{-i\phi_1}).\end{aligned} \tag{9}$$

Let $\rho(\phi)\exp(-i\Omega t)$ equal $-M$ times the line-charge perturbation of a single oscillating bunch. In terms of its Fourier components $\rho_n = (1/2\pi)\int_{-\pi}^{\pi} d\phi e^{-in\phi}\rho(\phi)$, the smoothed voltage induced by the oscillating charge is $\exp(-i\Omega t)\sum_{n=jM}\delta V_n e^{in\phi}$ (j = integer), where [15]

$$\delta V_n = -\omega_0 \rho_n Z(n\omega_0 + \Omega) \equiv -\omega_0 \rho_n Z_n. \tag{10}$$

Here, Z is the ring's total impedance and ω_0 is the ring's angular revolution frequency, related to the recirculation time T_0 by $\omega_0 = 2\pi/T_0$.

For bunches in a quadratic synchrotron potential affected by a slow rf oscillation ($\Omega\sigma_t \ll 1$), the line-charge perturbation caused by voltage perturbation $V(\phi, t) = \exp(-i\Omega t)\sum_{n=jM} V_n e^{in\phi}$ has been obtained from the Vlasov equation by Krinsky and Wang [3,15]. The Fourier components of the perturbation obey

$$\rho_m = \sum_{n=jM} \sum_{\mu=1}^{\infty} \left[\frac{T_{m,n}^{(\mu)}}{-\omega_0 Z_n}\right] V_n, \qquad j = \text{integer}. \tag{11}$$

The value of $T_{m,n}^{(\mu)}$ (including the effect of radiation damping) is [12]

$$T_{m,n}^{(\mu)} = -iZ_n\left[\frac{\alpha e {\omega_0}^2 I}{2\pi E {\omega_s}^2}\right]\frac{F_{m\omega_0}F_{n\omega_0}}{\mu!\, 2^{\mu-1}} \times \frac{m^\mu n^{\mu-1}(\omega_0\sigma_t)^{2\mu-2}}{1-(\Omega + i\mu\tau_L^{-1})^2/(\mu\omega_s)^2}, \tag{12}$$

where τ_L is the radiation damping time constant and $\tau_L^{-1} \ll \Omega$ is the radiation-damping rate. The momentum compaction is α, the magnitude of the electron charge is $e > 0$, the beam energy is E, the angular synchrotron frequency is ω_s, while $F_{m\omega_0} = \exp[-(m\omega_0\sigma_t)^2/2]$ is the bunch form factor at the angular frequency $m\omega_0$. For a voltage perturbation that is the sum of those from a line-charge oscillation and an rf-generator phase modulation ($V_n = \delta V_n + \Delta V_n$), retaining the dipole ($\mu = 1$) and quadrupole ($\mu = 2$) terms of Eq. (11) yields

$$\begin{aligned}\rho_m = &\sum_{n=jM} T_{m,n}^{(1)}\rho_n + \sum_{n=jM} T_{m,n}^{(2)}\rho_n \\ &+ \frac{T_{m,M}^{(1)}}{-\omega_0 Z_M}(\Delta V_M + \Delta V_{-M}) \\ &+ \frac{T_{m,M}^{(2)}}{-\omega_0 Z_M}(\Delta V_M - \Delta V_{-M}).\end{aligned} \tag{13}$$

Since $T_{m,n}^{(\mu)} = (m/n)^\mu (F_{m\omega_0}/F_{n\omega_0}) T_{n,n}^{(\mu)}$, Eq. (13) implies that

$$\begin{aligned}\rho_n &= nF_{n\omega_0}(A + nB + K + nL) \\ &\quad [\text{for } n = Mj,\ j = \text{integer}],\end{aligned} \tag{14}$$

where

$$\begin{aligned}A &\equiv \sum_n \frac{T_{n,n}^{(1)}\rho_n}{nF_{n\omega_0}} \qquad B \equiv \sum_n \frac{T_{n,n}^{(2)}\rho_n}{n^2 F_{n\omega_0}} \\ K &\equiv \frac{T_{m,M}^{(1)}}{-mF_{m\omega_0}\omega_0 Z_M}(\Delta V_M + \Delta V_{-M}) \\ &= \frac{i\alpha e I F_1}{T_0 E[\omega_s^2 - (\Omega + i\tau_L^{-1})^2]}(\Delta V_M + \Delta V_{-M}) \\ L &\equiv \frac{T_{m,M}^{(2)}}{-m^2 F_{m\omega_0}\omega_0 Z_M}(\Delta V_M - \Delta V_{-M}) \\ &= \frac{i\alpha e I F_1 M(\omega_0\sigma_t)^2}{T_0 E[4\omega_s^2 - (\Omega + 2i\tau_L^{-1})^2]}(\Delta V_M - \Delta V_{-M}).\end{aligned} \tag{15}$$

Substituting Eq. (14) into the expressions for A and B given by Eq. (15), we find that

$$\begin{aligned}A &= (A + K)\sum_n T_{n,n}^{(1)} + (B + L)\sum_n nT_{n,n}^{(1)} \\ B &= (A + K)\sum_n (T_{n,n}^{(2)}/n) + (B + L)\sum_n T_{n,n}^{(2)}.\end{aligned} \tag{16}$$

Solving Eq. (16) for A and B gives

$$\begin{aligned}A &= \frac{K[-\sum_n nT_{n,n}^{(1)}\sum_n (T_{n,n}^{(2)}/n) + \sum_n T_{n,n}^{(1)}(\sum_n T_{n,n}^{(2)} - 1)] - L\sum_n nT_{n,n}^{(1)}}{\sum_n nT_{n,n}^{(1)}\sum_n (T_{n,n}^{(2)}/n) - (\sum_n T_{n,n}^{(1)} - 1)(\sum_n T_{n,n}^{(2)} - 1)} \\ B &= \frac{L[-\sum_n nT_{n,n}^{(1)}\sum_n (T_{n,n}^{(2)}/n) + \sum_n T_{n,n}^{(2)}(\sum_n T_{n,n}^{(1)} - 1)] - K\sum_n (T_{n,n}^{(2)}/n)}{\sum_n nT_{n,n}^{(1)}\sum_n (T_{n,n}^{(2)}/n) - (\sum_n T_{n,n}^{(1)} - 1)(\sum_n T_{n,n}^{(2)} - 1)}.\end{aligned} \tag{17}$$

The line-charge perturbation $\rho(\phi)$ is related to $\rho_n = nF_{n\omega_0}(A + nB + K + nL)$ by $\rho_n \equiv (2\pi)^{-1}\int_{-\pi}^{\pi} d\phi\rho(\phi)\times \exp(-in\phi) \approx (2\pi)^{-1}\int_{-\infty}^{\infty} d\phi\rho(\phi)\exp(-in\phi)$, so that [22]

$$\rho(\phi) = \frac{\sqrt{2\pi}\exp(\frac{-\phi^2}{2(\omega_0\sigma_t)^2})}{(\omega_0\sigma_t)^3}\left[i(A + K)\phi + (B + L)\left(1 - \frac{\phi^2}{(\omega_0\sigma_t)^2}\right)\right]. \tag{18}$$

The general solution for the line-charge perturbation consists of the above driven oscillation at angular frequency Ω, plus any solution describing unforced Robinson oscillations. When Robinson oscillations are stable, unforced Robinson oscillations are damped transients that may be neglected.

Averaging over the electrons in a bunch gives [23]

$$\begin{aligned}\bar{\phi}(t) &= (IT_0)^{-1}\int_{-\pi}^{\pi} d\phi\,\phi\rho(\phi)\exp(-i\Omega t) \approx (IT_0)^{-1}\int_{-\infty}^{\infty} d\phi\,\phi\rho(\phi)\exp(-i\Omega t) = 2\pi i(A+K)(IT_0)^{-1}\\ &\quad\times\exp(-i\Omega t)\\ \overline{\phi^2}(t) - (\omega_0\sigma_t)^2 &= (IT_0)^{-1}\int_{-\pi}^{\pi} d\phi\,\phi^2\rho(\phi)\exp(-i\Omega t) \approx (IT_0)^{-1}\int_{-\infty}^{\infty} d\phi\,\phi^2\rho(\phi)\exp(-i\Omega t)\\ &= -4\pi(B+L)(IT_0)^{-1}\exp(-i\Omega t).\end{aligned} \tag{19}$$

The complex amplitude of the bunch's phase oscillation is

$$\Phi = \frac{2\pi i(A+K)}{IT_0} = \frac{2\pi i}{IT_0}\left[\frac{K(\sum_n T^{(2)}_{n,n} - 1) - L\sum_n nT^{(1)}_{n,n}}{\sum_n nT^{(1)}_{n,n}\sum_n(T^{(2)}_{n,n}/n) - (\sum_n T^{(1)}_{n,n} - 1)(\sum_n T^{(2)}_{n,n} - 1)}\right]. \tag{20}$$

In Eq. (20), the amplitude of the beam's longitudinal oscillation Φ is measured in ring phase, which varies from $-\pi$ to π around the ring, while the rf-generator phase modulation amplitude Ψ is measured in rf phase, which varies from $-M\pi$ to $M\pi$ around the ring. Letting $\Phi_{\rm rf} = M\Phi$ equal the amplitude of the beam oscillation measured in rf phase, we expand Eq. (20) to obtain the transfer function from generator phase modulation to beam phase modulation

$$\begin{aligned}G_0 \equiv \frac{\Phi_{\rm rf}}{\Psi} &= \frac{iM\pi\alpha eF_1}{T_0^2E[\sum_n nT^{(1)}_{n,n}\sum_n(T^{(2)}_{n,n}/n) - (\sum_n T^{(1)}_{n,n} - 1)(\sum_n T^{(2)}_{n,n} - 1)]}\\ &\times\left\{\frac{(\sum_n T^{(2)}_{n,n} - 1)}{\omega_s^2 - (\Omega + i\tau_L^{-1})^2}\left[\frac{\cos\phi_{1+}e^{i\phi_{1+}}}{\cos\phi_1 e^{i\phi_1}}(V_{T1}e^{-i\psi_1} + 2IR_1F_1\cos\phi_1 e^{i\phi_1})\right.\right.\\ &\left.-\frac{\cos\phi_{1-}e^{-i\phi_{1-}}}{\cos\phi_1 e^{-i\phi_1}}(V_{T1}e^{i\psi_1} + 2IR_1F_1\cos\phi_1 e^{-i\phi_1})\right]\\ &-\frac{M(\omega_0\sigma_t)^2\sum_n nT^{(1)}_{n,n}}{4\omega_s{}^2 - (\Omega + 2i\tau_L{}^{-1})^2}\left[\frac{\cos\phi_{1+}e^{i\phi_{1+}}}{\cos\phi_1 e^{i\phi_1}}(V_{T1}e^{-i\psi_1} + 2IR_1F_1\cos\phi_1 e^{i\phi_1})\right.\\ &\left.\left.+\frac{\cos\phi_{1-}e^{-i\phi_{1-}}}{\cos\phi_1 e^{-i\phi_1}}(V_{T1}e^{i\psi_1} + 2IR_1F_1\cos\phi_1 e^{-i\phi_1})\right]\right\}.\end{aligned} \tag{21}$$

When phase feedback is utilized, the generator phase-modulation amplitude Ψ depends upon the beam oscillation amplitude $\Phi_{\rm rf}$. For ideal phase feedback that suppresses Robinson-dipole oscillations, a proportion g of the bunch's energy error $\bar{\varepsilon}(t)$ is removed on each turn, so that the rf voltage perturbation from feedback obeys $eF_1\Delta V_f(\phi = 0, t) = -g\bar{\varepsilon}(t)$. An electron's longitudinal coordinate ϕ and energy error ε are related by $\omega_0^{-1}d\phi/dt = -\alpha\varepsilon/E$, so that an oscillation with angular frequency Ω obeys $d\bar{\phi}(t)/dt = -i\Omega\bar{\phi}(t) = -\omega_0\alpha\bar{\varepsilon}(t)/E$. Thus,

$$\Delta V_f(\phi = 0, t) = -\frac{ig\Omega\Phi E}{F_1 e\alpha\omega_0}\exp(-i\Omega t) = -\frac{ig\Omega\Phi_{\rm rf}E}{F_1 e\alpha\omega_g}\exp(-i\Omega t). \tag{22}$$

For phase feedback, $\Delta V_f(\phi = 0, t)$ equals $(\Delta V_M + \Delta V_{-M})\exp(-i\Omega t)$, where ΔV_M and ΔV_{-M} are given by evaluating Eq. (9) with $\Psi = \psi_f$. Relating ψ_f to $\Phi_{\rm rf}$ gives the feedback response

$$\begin{aligned}H_f &\equiv \frac{\psi_f}{\Phi_{\rm rf}}\\ &= \frac{gE\Omega T_0}{M\pi F_1 e\alpha}\left[\frac{\cos\phi_{1+}e^{i\phi_{1+}}}{\cos\phi_1 e^{i\phi_1}}(V_{T1}e^{-i\psi_1} + 2IR_1F_1\cos\phi_1 e^{i\phi_1}) - \frac{\cos\phi_{1-}e^{-i\phi_{1-}}}{\cos\phi_1 e^{-i\phi_1}}(V_{T1}e^{i\psi_1} + 2IR_1F_1\cos\phi_1 e^{-i\phi_1})\right]^{-1}.\end{aligned} \tag{23}$$

Letting $\Psi = \psi_g + \psi_f$ in Eq. (21), where ψ_f is given by Eq. (23), we solve for the transfer function from generator-noise phase modulation to beam phase modulation G_f obtaining

$$G_f \equiv \frac{\Phi_{\rm rf}}{\psi_g} = \frac{1}{G_0^{-1} - H_f}, \tag{24}$$

where G_0 and H_f are given by Eqs. (21) and (23). An analogous equation giving $\overline{\phi^2}(t)$ in the presence of ideal phase feedback may be obtained by substituting $\Psi = \psi_g + \psi_f = \psi_g(1 + H_f G_f)$ in the second equation of Eq. (19).

When there is little coupling between dipole and quadrupole Robinson modes, the dipole-mode peak is described by the dipole-mode approximation to G_f, obtained by neglecting terms in Eq. (24) whose denominator is $4{\omega_s}^2 - (\Omega + 2i{\tau_L}^{-1})^2$:

$$G_{fD} = \frac{(\frac{i\pi M\alpha e F_1}{ET_0^2})[\frac{\cos\phi_{1+}e^{i\phi_{1+}}}{\cos\phi_1 e^{i\phi_1}}(V_{T1}e^{-i\psi_1} + 2IR_1F_1\cos\phi_1 e^{i\phi_1}) - \frac{\cos\phi_{1-}e^{-i\phi_{1-}}}{\cos\phi_1 e^{-i\phi_1}}(V_{T1}e^{i\psi_1} + 2IR_1F_1\cos\phi_1 e^{-i\phi_1})]}{-\frac{ig\Omega}{T_0} - (\sum_n T_{n,n}^{(1)} - 1)[\omega_s^2 - (\Omega + i\tau_L^{-1})^2]}. \tag{25}$$

For $g/2T_0 \ll \Omega$, the denominator of Eq. (25) is approximately

$$-\left(\sum_n \hat{T}_{n,n}^{(1)} - 1\right)\left[{\omega_s}^2 - \left(\Omega + i{\tau_L}^{-1} + i\frac{g}{2T_0}\right)^2\right], \tag{26}$$

where $\hat{T}_{n,n}^{(1)}$ is obtained by substituting $\tau_L^{-1} + g/(2T_0)$ for τ_L^{-1} in $T_{n,n}^{(1)}$. Acting on the dipole mode, the feedback is equivalent to an increase in the radiation-damping rate by $g/(2T_0)$. Thus, the feedback damps the dipole mode with time constant

$$\tau_f = 2T_0/g. \tag{27}$$

III. COMPARISON WITH EXPERIMENT

To compare the calculated transfer function G_f with experiment, the longitudinal phase transfer function in the Aladdin 800-MeV electron storage ring was measured while operating in the standard low-emittance lattice [9]. Ring parameters are shown in Table I.

A Stanford Research Systems Model SR780 2-channel network signal analyzer was used to measure the longitudinal transfer function for frequencies of 500–6000 Hz. The analyzer's source signal was input to a phase modulator circuit, in which the signal passes through two high-pass filters with cutoff frequency of 150 Hz and one low-pass filter with cutoff frequency of 8200 Hz. The beam phase response was measured with a phase detector circuit where one input is the master oscillator signal; the other input is the sum of the voltages induced by the beam upon two 0.45-m striplines, bandpass filtered at the rf frequency. The beam response signal was input to the analyzer, which computes the amplitude and phase of the longitudinal beam transfer function versus frequency. For each measurement, we exponentially averaged 200 spectra using the fast Fourier transform method. Changing the signal voltage by a factor of 4 did not affect the results. To correct for the two high-pass filters and the one low-pass filter, the experimental transfer function at angular frequency Ω

TABLE I. Parameters for the Aladdin low-emittance LF15 lattice. The shunt impedance value equals the resistance of the equivalent parallel *RLC* circuit, and is equal to one-half of the linac definition of shunt impedance.

Parameter	Symbol	Aladdin low-emittance lattice
Ring energy	E	800 MeV
Natural relative energy spread	$\sigma_{E\,\rm nat}/E$	4.8×10^{-4}
Synchronous voltage	V_s	17.4 kV
Recirculation time	T_0	2.96×10^{-7} s
Number of bunches	M	15
Fundamental cavity shunt impedance	$R_1{}^\circ$ (unloaded)	0.5 MΩ
Fundamental cavity quality factor	$Q_1{}^\circ$ (unloaded)	8000
Fundamental cavity coupling coefficient	β_1	11
Harmonic-cavity harmonic number	ν	4
Harmonic-cavity shunt impedance	$R_2{}^\circ$ (unloaded)	1.24 MΩ
Harmonic-cavity quality factor	$Q_2{}^\circ$ (unloaded)	20 250
Harmonic-cavity coupling coefficient	β_2	1.5
Fundamental cavity maximum voltage	V_{T1}	50 kV
Fundamental cavity loadangle	$\theta_{\rm v1}$	0 degrees
Momentum compaction	α	0.0054
Radiation-damping time constant	τ_L	13.5 ms

was multiplied by $[(-i\Omega + 2\pi \cdot 150)/(-i\Omega)]^2[(-i\Omega + 2\pi \cdot 8200)/(2\pi \cdot 8200)]$. No additional frequency limitations from the rf system are expected.

To vary the contribution of the coupled-quadrupole Robinson mode to the transfer function, we "tune in" the harmonic cavity; i.e., we decrease its resonant frequency, which slightly exceeds the fourth harmonic of the 50.582 MHz rf frequency. This increases the harmonic cavity voltage, decreases the synchrotron frequency, and increases the bunchlength. Tuning in the cavity so that the synchrotron frequency is zero is referred to as "optimal bunchlengthening" with an "optimal" harmonic-cavity voltage and a "flattop" bunch shape. If the harmonic cavity is tuned in further, the result is "double-hump" bunches (with two density peaks) confined in a synchrotron potential with two minima [12,18]. For low harmonic-cavity voltages, parasitic coupled-bunch instabilities are driven by higher-order modes in the rf cavities. When the harmonic-cavity voltage exceeds ~70% of its optimal voltage, nonquadratic contributions to the synchrotron potential provide Landau damping that suppresses the coupled-bunch instabilities [5].

As the harmonic cavity is tuned in, the coupled quadrupole-mode frequency decreases, while the coupled dipole Robinson mode frequency remains nearly constant at 2.9 kHz. [According to Eqs. (9) and (41) of Ref. [16], tuning in a harmonic cavity has little effect upon the dipole-mode Robinson frequency when the dipole-mode angular frequency is $\ll \omega_2/2Q_2$, where ω_2 and Q_2 are the resonant angular frequency and quality factor of the harmonic cavity.] When the harmonic-cavity voltage reaches 85% of its optimal value, the coupled quadrupole frequency equals the coupled dipole frequency, resulting in a fast mode-coupling instability [5,6]. This instability prevents stable operation with optimally lengthened bunches. When the harmonic-cavity voltage equals 110%–130% of its optimal voltage, the double-hump bunches are stable; the coupled quadrupole frequency increases with harmonic-cavity voltage in this regime. Standard ring operation employs stable double-hump bunches with harmonic-cavity voltage equaling 120% of the optimal voltage. To reduce noise in our infrared beam line, dipole Robinson oscillations are suppressed with phase feedback [6,9,12,13].

When a harmonic cavity stretches the bunch, the computed transfer function G_f given by Eq. (24) applies to stable bunches, provided that the synchrotron potential is approximately quadratic. We have previously found that Robinson oscillations of highly stretched bunches in nonquadratic synchrotron potentials with a single minimum may also be approximately modeled if the calculated rigid-dipole oscillation frequency ω_R is substituted for the synchrotron frequency ω_s in $T^{(\mu)}_{m,n}$ [5]. Since ω_R equals ω_s for a quadratic synchrotron potential, this substitution has no effect for bunches in a quadratic synchrotron potential and negligible effect for bunches that are not highly stretched. While this substitution approximates the coherent frequencies of Robinson modes in a highly stretched bunch within ~10%, it does not model the Landau damping from the nonquadratic potential. To describe our experimental results, we calculate the transfer functions G_0 and G_f by using formulas in Appendix A to evaluate Eqs. (21) and (24) with ω_R substituted for ω_s.

A. Robinson-stable bunches in synchrotron potentials with a single minimum

Figure 1(a) shows the amplitude of the phase transfer function for a ring current of 166 mA and a low harmonic-cavity voltage equaling 22% of its optimal voltage. The beam undergoes parasitic coupled-bunch instabilities while Robinson modes are stable. Measured transfer function amplitudes are shown for ring operation without and with Robinson-dipole feedback, which suppresses the phase noise peak at 2.9 kHz by 20 dB.

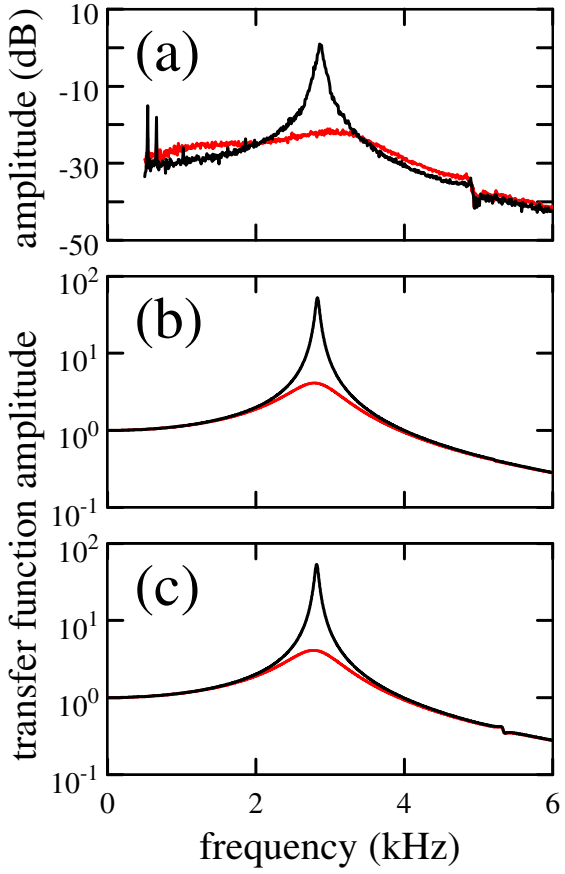

FIG. 1. (Color) Operation with passive harmonic-cavity voltage equaling 22% of that required for optimal bunch lengthening. Black curves: phase feedback off. Red curves: phase feedback on. (a) Experimental measurement of the transfer function amplitude. (b) Transfer function amplitude calculated with the beam energy spread equaling its natural value. (c) Transfer function amplitude calculated with the beam energy spread equaling 3 times its natural value.

Using a computer code that models a harmonic cavity [5], we computed the harmonic-cavity tuning angle ($\phi_2 = -89.1°$), synchronous phase ($\psi_1 = 69.6°$), bunchlength ($\sigma_t = 158$ ps), and bunch form factors in the two rf cavities ($F_1 = 0.999$, $F_2 = 0.980$). We also computed the tuning angle of the fundamental cavity ($\phi_1 = 14.5°$), which is operated in the "compensated condition" with generator current in phase with the cavity voltage [19]. With these computed values, we evaluate the transfer function G_f. We model our Robinson-dipole feedback with a damping time constant $\tau_f = 2T_0/g$ of 0.5 ms, which reduces the peak value of $|G_f|$ by a factor of 10, in agreement with the experimental 20-dB reduction in the transfer function amplitude. This value of τ_f is consistent with simulations that suggest $0.3 \text{ ms} \leq \tau_f \leq 0.5$ ms [6,12,13]. The calculated transfer function amplitude $|G_f|$ is displayed in Fig. 1(b) as a function of frequency $\Omega/2\pi$. Peaks are seen at the coupled dipole and quadrupole Robinson mode frequencies.

The reasonable agreement between Figs. 1(a) and 1(b) confirms the applicability of the calculated transfer function G_f. However, the calculated peak at the coupled quadrupole frequency is much smaller than the measured peak.

Since parasitic coupled-bunch instabilities are not suppressed with a low harmonic-cavity voltage, the beam's energy spread exceeds its natural value. In simulations of a typical higher-order mode, the energy spread is increased by a factor of 2–4 when the harmonic-cavity voltage is much less than optimal [24]. To include this effect, we recalculated the transfer functions for energy spread equaling 3 times the natural value. The increased energy spread causes a longer bunchlength, resulting in a larger peak at the coupled quadrupole frequency. The recalculated transfer function amplitudes, shown in Fig. 1(c), are in better agreement with the measurements.

Figure 2(a) displays the measured transfer function phase shift in the usual convention where a negative phase

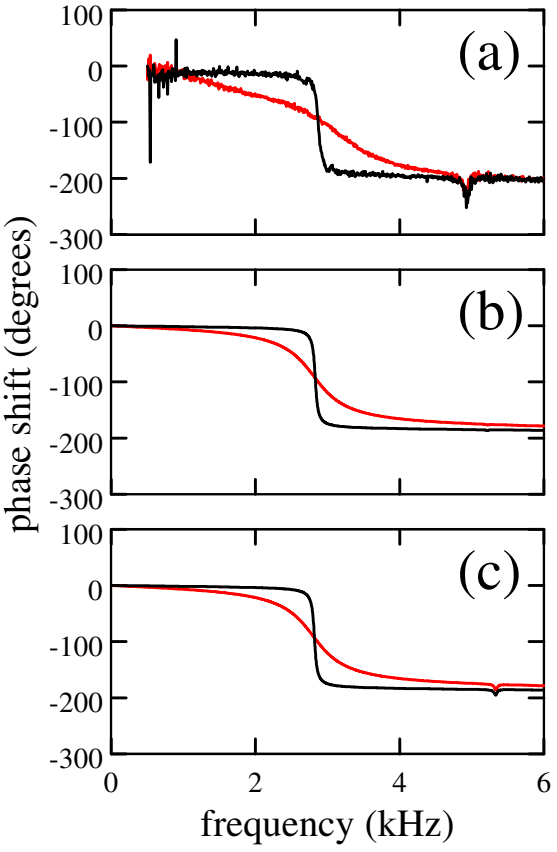

FIG. 2. (Color) Operation with passive harmonic-cavity voltage equaling 22% of that required for optimal bunch lengthening. Black curves: phase feedback off. Red curves: phase feedback on. (a) Experimental measurement of the transfer function phase shift. (b) Phase shift calculated with the beam energy spread equaling its natural value. (c) Phase shift calculated with the beam energy spread equaling 3 times its natural value.

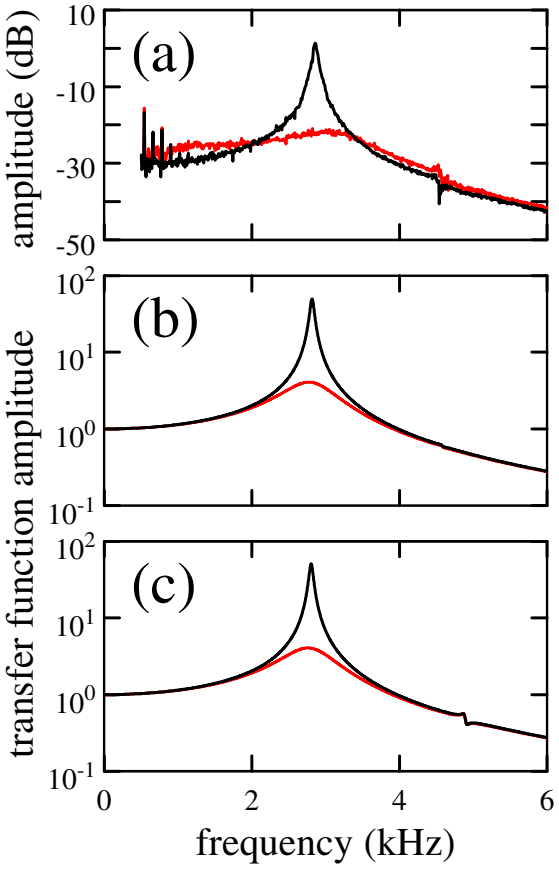

FIG. 3. (Color) Operation with passive harmonic-cavity voltage equaling 41% of that required for optimal bunch lengthening. Black curves: phase feedback off. Red curves: phase feedback on. (a) Experimental measurement of the transfer function amplitude. (b) Transfer function amplitude calculated with the beam energy spread equaling its natural value. (c) Transfer function amplitude calculated with the beam energy spread equaling 3 times its natural value.

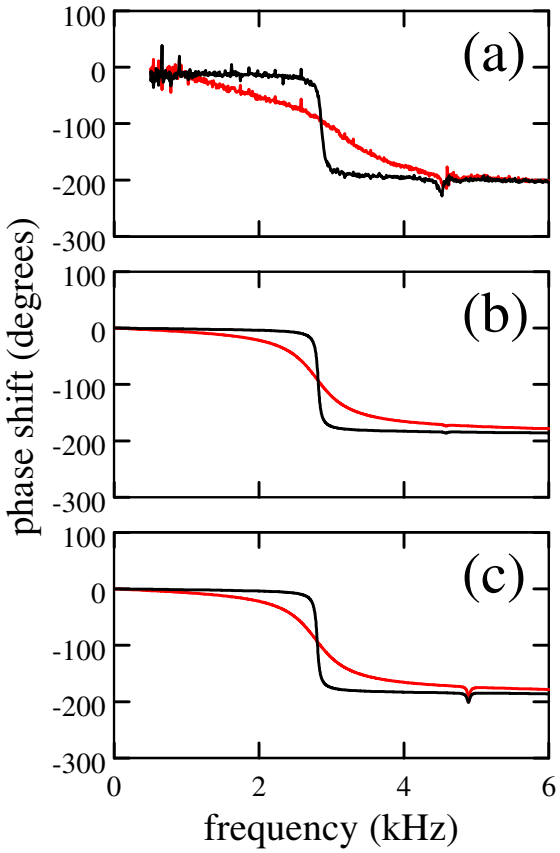

FIG. 4. (Color) Operation with passive harmonic-cavity voltage equaling 41% of that required for optimal bunch lengthening. Black curves: phase feedback off. Red curves: phase feedback on. (a) Experimental measurement of the transfer function phase shift. (b) Phase shift calculated with the beam energy spread equaling its natural value. (c) Phase shift calculated with the beam energy spread equaling 3 times its natural value.

describes a phase lag of the beam response. Since we have considered an excitation of the form $\exp(-i\Omega t)$, the phase shift is the opposite of the phase of our transfer function. For comparison, the calculated phase shift is shown in Fig. 2(b), while Fig. 2(c) shows the recalculated phase shift for energy spread equaling 3 times its natural value.

The amplitude and phase shift calculations are both consistent with the ring's energy spread exceeding its natural value as a result of parasitic coupled-bunch instability.

Figures 3(a) and 3(b) show measured and calculated transfer function amplitude with a larger harmonic-cavity voltage equaling 41% of its optimal voltage, for a ring current of 176 mA. Again, the beam undergoes parasitic coupled-bunch instabilities while Robinson modes are stable. The coupled-quadrupole peak is observed at lower frequency than in Fig. 1. To model the energy spread caused by the parasitic coupled-bunch instabilities, we recalculated the transfer functions for energy spread equaling 3 times the natural value. The recalculated transfer function amplitudes, shown in Fig. 3(c), are in good agreement with the measurements.

Figure 4 shows the measured and calculated phase shifts for harmonic-cavity voltage equaling 41% of its optimal value. The amplitude and phase shift calculations are both consistent with the ring's energy spread equaling about 3 times its natural value as a result of parasitic coupled-bunch instability.

Figure 5(a) shows the measured transfer function amplitude with a harmonic-cavity voltage equaling 74% of its optimal voltage, for a ring current of 178 mA. Robinson modes and parasitic coupled-bunch modes are stable, so that the beam's energy spread is expected to equal its natural value. Since the coupled quadrupole frequency is only 20% higher than that of the coupled dipole mode, dipole-quadrupole-mode coupling has a large effect upon the transfer function. The feedback suppresses the coupled-dipole peak with little effect upon the peak at the coupled quadrupole frequency. With feedback, the transfer function has largest amplitude at the coupled-quadrupole frequency. The calculated transfer function amplitude, shown in Fig. 5(b), agrees with the measured amplitude.

Figure 6 shows the measured and calculated phase shifts for harmonic-cavity voltage equaling 74% of the optimal voltage. The measurements are again in agreement with the analytic modeling.

For Robinson-stable bunches in synchrotron potentials with a single minimum, the beam phase noise was measured while operating with an rf generator whose phase

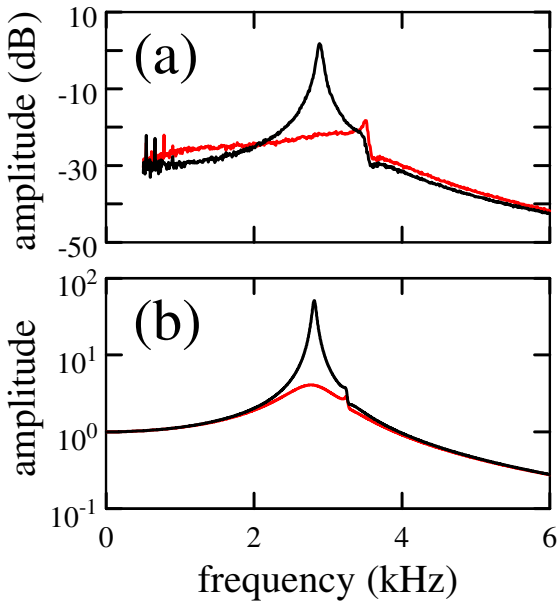

FIG. 5. (Color) Operation with passive harmonic-cavity voltage equaling 74% of that required for optimal bunch lengthening. Black curves: phase feedback off. Red curves: phase feedback on. (a) Experimental measurement of the transfer function amplitude. (b) Transfer function amplitude calculated with the beam energy spread equaling its natural value.

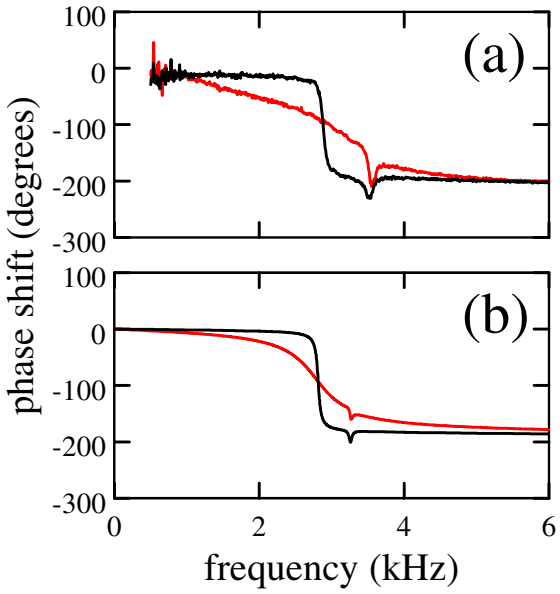

FIG. 6. (Color) Operation with passive harmonic-cavity voltage equaling 74% of that required for optimal bunch lengthening. Black curves: phase feedback off. Red curves: phase feedback on. (a) Experimental measurement of the transfer function phase shift. (b) Phase shift calculated with the beam energy spread equaling its natural value.

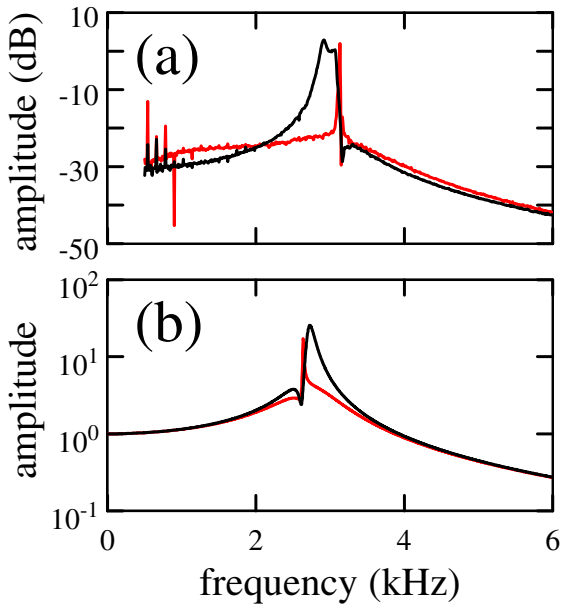

FIG. 7. (Color) Operation with optimal bunch lengthening, where a fast mode-coupling Robinson instability increases the beam's phase noise and energy spread. Black curves: phase feedback off. Red curves: phase feedback on. (a) Experimental measurement of the transfer function amplitude. (b) Transfer function amplitude calculated with the beam energy spread equaling its natural value.

noise is approximately white noise between 500 Hz and 6 kHz. As expected, the spectra of measured phase noise are similar to the amplitudes of the measured transfer functions.

B. Robinson-unstable and double-hump bunches

Robinson-unstable and double-hump bunches do not satisfy the assumptions of our analytic model, which describes Robinson-stable bunches in an approximately quadratic synchrotron potential. Consequently, the measured transfer function may not agree with our calculated transfer function.

At ring current of 182 mA, optimally lengthened bunches are destabilized by the fast mode-coupling Robinson instability, which results in a beam oscillation at 2.9 kHz. Measurements of beam dimensions and results of simulations suggest that the energy spread exceeds the natural value by about 40% without phase feedback and 0%–5% with phase feedback. Figure 7(a) shows the measured transfer function amplitudes with and without phase feedback. The narrow peak corresponding to coupled quadrupole motion is not suppressed by the feedback.

The calculated transfer function amplitudes are shown in Fig. 7(b). As in the measurements, the narrow peak corresponding to coupled quadrupole motion is not suppressed by the feedback. In the calculations, the frequency of the narrow peak is lower than that of the dipole peak, differing from the measurements. This discrepancy may result from the presence of fast mode-coupling Robinson instability,

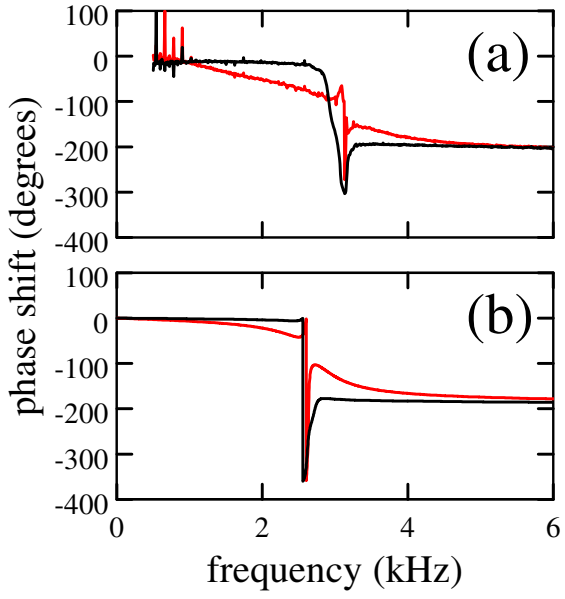

FIG. 8. (Color) Operation with optimal bunch lengthening, where a fast mode-coupling Robinson instability increases the beam's phase noise and energy spread. Black curves: phase feedback off. Red curves: phase feedback on. (a) Experimental measurement of the transfer function phase shift. (b) Phase shift calculated with the beam energy spread equaling its natural value.

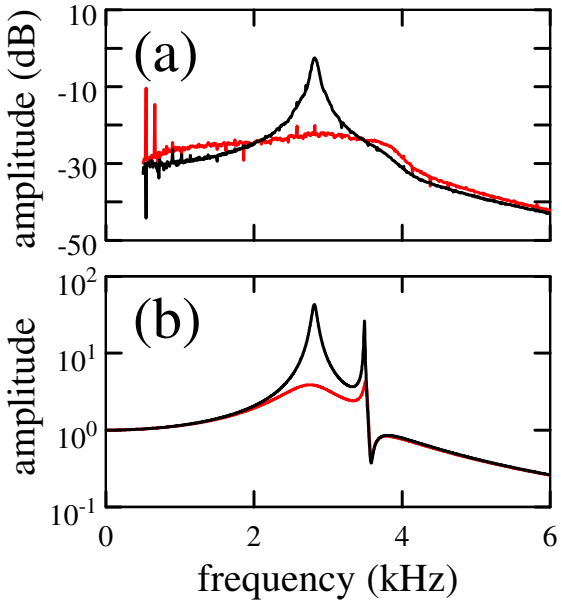

FIG. 9. (Color) Operation with passive harmonic-cavity voltage equaling 119% of that required for optimal bunch lengthening. In this case, a double-hump bunch is confined in a synchrotron potential with two minima. Black curves: phase feedback off. Red curves: phase feedback on. (a) Experimental measurement of the transfer function amplitude. (b) Transfer function amplitude calculated with the beam energy spread equaling its natural value.

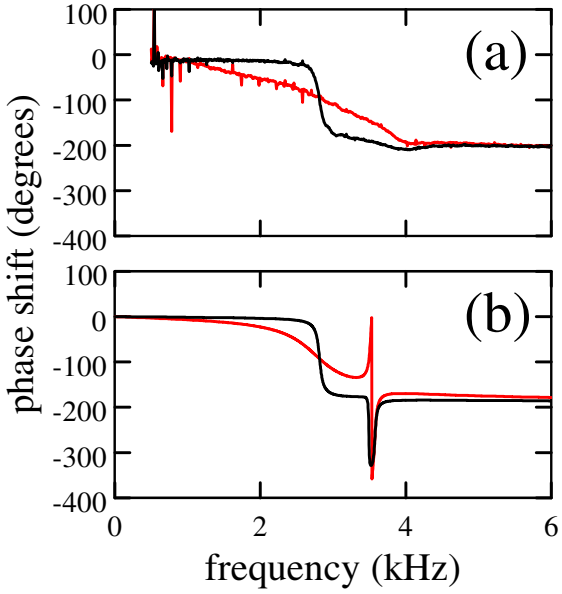

FIG. 10. (Color) Operation with passive harmonic-cavity voltage equaling 119% of that required for optimal bunch lengthening. In this case, a double-hump bunch is confined in a synchrotron potential with two minima. Black curves: phase feedback off. Red curves: phase feedback on. (a) Experimental measurement of the transfer function phase shift. (b) Phase shift calculated with the beam energy spread equaling its natural value.

inaccuracy in the parameters used for modeling, and/or inaccuracy in applying the analytical model to optimally lengthened bunches.

Figure 8 shows the measured and calculated phase shifts for unstable optimally lengthened bunches. Approximate agreement is obtained.

For unstable optimally lengthened bunches, the phase noise spectrum was measured while operating with an rf generator whose phase noise is approximately white noise between 500 Hz and 6 kHz. In the spectra of beam phase noise, the peak at 2.9 kHz is about 10 dB higher than that of the measured transfer function. This suggests that the beam phase oscillations include unstable Robinson oscillations in addition to driven Robinson oscillations from the rf generator noise.

Figure 9 shows measured and calculated transfer function amplitudes for stable double-hump bunches with harmonic-cavity voltage equaling 119% of the optimal value, at a ring current of 191 mA. The measurements and calculations differ for frequencies near the coupled quadrupole-mode frequency, where the measurements show a much broader peak. The discrepancy in the quadrupole-peak width may result from the neglect of Landau damping in the calculations.

Figure 10 shows the measured and calculated phase shifts for double-hump bunches when the harmonic-cavity voltage is 119% of the optimal voltage. Again, the measurements show a much broader feature at the coupled quadrupole frequency.

For double-hump bunches, the beam phase noise was measured while operating with an rf generator whose phase noise is approximately white noise between 500 Hz and 6 kHz. As expected, the spectrum of measured phase noise is similar to the amplitude of the measured transfer function.

For double-hump bunches, the synchrotron potential well has two minima, strongly violating our assumption of an approximately quadratic synchrotron potential well. Nonetheless, the analytic model gives good predictions of the frequencies of the coupled dipole and quadrupole-mode peaks, as well as the dipole peak width.

For Robinson-unstable and double-hump bunches, macroparticle simulations more accurately model the beam noise and its suppression by feedback [6,12,13].

IV. SUMMARY

In an electron storage ring, the rf generator phase noise drives longitudinal beam oscillations. In this article, we include the coupled dipole and quadrupole Robinson modes when calculating the driven beam motion in a quadratic synchrotron potential. We obtain the transfer function from generator-noise phase modulation to beam phase modulation. Because of mode coupling, two peaks occur in the transfer function and in the spectrum of the

beam's longitudinal phase noise—a large peak at the coupled dipole mode resonant frequency and a smaller peak at the coupled quadrupole-mode resonant frequency.

For Robinson-stable bunches in a synchrotron potential with a single minimum, comparison with experiment confirms the validity of our analytic formula for the transfer function. The modification of the transfer function by dipole-quadrupole-mode coupling and feedback is well described. The calculated transfer function is useful in evaluating the phase feedback that is required for quiet operation of the Aladdin infrared beam line.

ACKNOWLEDGMENTS

The authors thank J. J. Bisognano, M. A. Green, and K. D. Jacobs for valuable discussions, and R. A. Legg for experimental assistance. This work is based upon research conducted at the Synchrotron Radiation Center, University of Wisconsin-Madison, which is supported by the National Science Foundation under Award No. DMR-0537588.

APPENDIX A: rf SYSTEM WITH PASSIVE HARMONIC CAVITY

Consider an rf system with a fundamental cavity whose resonant frequency is close to the rf-generator angular frequency ω_g, and passive harmonic cavity whose resonant frequency is close to $\nu\omega_g$, where the integer ν is the harmonic number of the passive cavity. Let R_1, Q_1, ω_1, and F_1 denote the resonant impedance, quality factor, resonant angular frequency, and bunch form factor of the fundamental rf cavity, while R_2, Q_2, ω_2, and F_2 describe the harmonic cavity. The values R_1 and Q_1 describe the effective impedance of the loaded fundamental cavity, equaling $1/(1+\beta_1)$ times the unloaded values, where β_1 is the rf coupling coefficient of the fundamental cavity. Similarly, R_2 and Q_2 describe the loaded harmonic cavity, equaling $1/(1+\beta_2)$ times the unloaded values, where β_2 is the harmonic cavity's rf coupling coefficient.

Our definitions of the rf cavities' tuning angles are $\tan\phi_1 = 2Q_1(\omega_g - \omega_1)/\omega_1$ and $\tan\phi_2 = 2Q_2(\nu\omega_g - \omega_2)/\omega_2$. For angular oscillation frequency Ω, we define sideband tuning angles $\phi_{1\pm}$ and $\phi_{2\pm}$ by $\tan\phi_{1\pm} = 2Q_1(\omega_g \pm \Omega - \omega_1)/\omega_1$ and $\tan\phi_{2\pm} = 2Q_2(\nu\omega_g \pm \Omega - \omega_2)/\omega_2$. To evaluate Eqs. (21)–(26) with the rigid-dipole oscillation frequency ω_R substituted for ω_s, we use the following relations to describe the dominant modes of the rf cavities [5]. A ring without a harmonic cavity is described by $R_2 = 0$.

$$\omega_R{}^2 = \frac{\alpha e\omega_g}{ET_o}(F_1 V_{T1}\sin\psi_1 + \nu I F_2{}^2 R_2 \sin 2\phi_2) \tag{A1}$$

$$\sum_n T^{(1)}_{n,n} = \frac{\alpha e\omega_g I}{2ET_0[\omega_R^2 - (\Omega + i\tau_L^{-1})^2]}[R_1F_1^2(\sin2\phi_{1-} + \sin2\phi_{1+} + 2i\cos^2\phi_{1-} - 2i\cos^2\phi_{1+}) + \nu R_2F_2^2(\sin2\phi_{2-} + \sin2\phi_{2+} + 2i\cos^2\phi_{2-} - 2i\cos^2\phi_{2+})] \tag{A2}$$

$$\sum_n T^{(2)}_{n,n} = \frac{\alpha e\omega_g I(\omega_g\sigma_t)^2}{2ET_0[4\omega_R^2 - (\Omega + 2i\tau_L^{-1})^2]}[R_1F_1^2(\sin2\phi_{1-} + \sin2\phi_{1+} + 2i\cos^2\phi_{1-} - 2i\cos^2\phi_{1+}) + \nu^3 R_2F_2^2(\sin2\phi_{2-} + \sin2\phi_{2+} + 2i\cos^2\phi_{2-} - 2i\cos^2\phi_{2+})] \tag{A3}$$

$$\sum_n nT^{(1)}_{n,n} = \frac{-M\alpha e\omega_g I}{2ET_0[\omega_R^2 - (\Omega + i\tau_L^{-1})^2]}[R_1F_1^2(\sin2\phi_{1-} - \sin2\phi_{1+} + 2i\cos^2\phi_{1-} + 2i\cos^2\phi_{1+}) + \nu^2 R_2F_2^2(\sin2\phi_{2-} - \sin2\phi_{2+} + 2i\cos^2\phi_{2-} + 2i\cos^2\phi_{2+})] \tag{A4}$$

$$\sum_n (T^{(2)}_{n,n}/n) = \frac{-\alpha e\omega_g I(\omega_g\sigma_t)^2}{2MET_0[4\omega_R^2 - (\Omega + 2i\tau_L^{-1})^2]}[R_1F_1^2(\sin2\phi_{1-} - \sin2\phi_{1+} + 2i\cos^2\phi_{1-} + 2i\cos^2\phi_{1+}) + \nu^2 R_2F_2^2(\sin2\phi_{2-} - \sin2\phi_{2+} + 2i\cos^2\phi_{2-} + 2i\cos^2\phi_{2+})]. \tag{A5}$$

[1] J. M. Byrd, in *Proceedings of the 1999 Particle Accelerator Conference, New York* (IEEE, Piscataway, NJ, 1999), p. 1806.

[2] J. M. Byrd, M. Martin, and W. McKinney, in Ref. [1], p. 495.

[3] J. M. Wang, in *Physics of Particle Accelerators*, edited by M. Month and M. Dienes, AIP Conf. Proc. No. 153 (AIP, New York, 1987), p. 697.

[4] Tai-Sen F. Wang, Part. Accel. **34**, 105 (1990).

[5] R. A. Bosch, K. J. Kleman, and J. J. Bisognano, Phys. Rev. ST Accel. Beams **4**, 074401 (2001).

[6] R. A. Bosch, K. J. Kleman, and J. J. Bisognano, in *Proceedings of the 2003 Particle Accelerator*

Conference, Portland, OR (IEEE, Piscataway, NJ, 2003), p. 3147.
[7] R. A. Bosch, Synchrotron Radiation Center Technical Note No. SRC-202, 2003.
[8] R. A. Bosch and R. L. Julian, Rev. Sci. Instrum. **73**, 1420 (2002).
[9] K. D. Jacobs, R. A. Bosch, D. E. Eisert, M. V. Fisher, M. A. Green, R. G. Keil, K. J. Kleman, R. A. Legg, J. P. Stott, and W. S. Trzeciak, in Ref. [6], p. 887.
[10] M. Hara, T. Nakamura, T. Ohshima, and T. Takashima, in *Proceedings of the Sixth European Particle Accelerator Conference, Stockholm* (IOP, Bristol, 1998), p. 1280.
[11] T. Ohshima and N. Kumagai, in *Proceedings of the 2001 Particle Accelerator Conference, Chicago* (IEEE, Piscataway, NJ, 2001), p. 1975.
[12] R. A. Bosch, K. D. Jacobs, and K. J. Kleman, in *Proceedings of the 2005 Particle Accelerator Conference, Knoxville, TN* (IEEE, Piscataway, NJ, 2005), p. 1180.
[13] R. A. Bosch, K. J. Kleman, and K. D. Jacobs, Synchrotron Radiation Center Technical Note No. SRC-204, 2003.
[14] A. Hofmann and S. Myers, in *Proceedings of the 11th International Conference on High Energy Accelerators, Geneva* (Birkhäuser Verlag, Basel, 1980), p. 610.
[15] S. Krinsky and J. M. Wang, Part. Accel. **17**, 109 (1985).
[16] R. A. Bosch and C. S. Hsue, Part. Accel. **42**, 81 (1993).
[17] K. J. Kleman, in *Proceedings of the 1995 Particle Accelerator Conference, Dallas* (IEEE, Piscataway, NJ, 1996), p. 1785.
[18] G. Penco and M. Svandrlik, Phys. Rev. ST Accel. Beams **9**, 044401 (2006).
[19] M. Sands, Institut National de Physique Nucleaire et de Physique des Particules, Technical Reports No. 2-76, 3-76, and 4-76, 1976.
[20] P. Marchand, Part. Accel. **36**, 205 (1992).
[21] P. B. Wilson, in *Physics of High Energy Particle Accelerators*, edited by R. A. Carrigan, F. R. Huson, and M. Month, AIP Conf. Proc. No. 87 (AIP, New York, 1982), p. 450.
[22] I. S. Gradshteyn and I. M. Ryzhik, *Table of Integrals, Series, and Products* (Academic Press, San Diego, 1994), 5th ed., p. 844, Eq. 7.376.1.
[23] Table of Integrals, Series, and Products (Ref. [22]), p. 382, Eq. 3.461.2.
[24] R. A. Bosch, Phys. Rev. ST Accel. Beams **8**, 084401 (2005).